

Research Article

Coupled Nanomechanical and Raman Microspectroscopic Investigation of Human Third Molar DEJ

**R. R. Gallagher,¹ M. Balooch,^{2,3} G. Balooch,² R. S. Wilson,³
S. J. Marshall,^{1,2,3} and G. W. Marshall^{1,2,3}**

¹Joint Graduate Group in Bioengineering, University of California at San Francisco and Berkeley,
San Francisco and Berkeley, CA 94143, USA

²Graduate Group in Oral and Craniofacial Sciences, University of California, San Francisco, CA 94143, USA

³Department of Preventive and Restorative Dental Sciences, University of California, San Francisco,
CA 94143-0758, USA

Correspondence should be addressed to G. W. Marshall, gw.marshall@ucsf.edu

Received 3 March 2009; Accepted 6 July 2009

Recommended by Spiros Zinelis

The dentino-enamel junction (DEJ) connects enamel, that covers the outer surface of a tooth, to a thicker underlying dentin. The DEJ is a critical interface that permits joining these materials that have widely dissimilar mechanical properties. AFM-based nanoindentation and Raman microspectroscopy were used to define the width and composition of human molar DEJ. Indentation elastic modulus and hardness of enamel, dentin, and DEJ were determined along lines of indents made at $2\ \mu\text{m}$ intervals across the DEJ. Indents made at maximum loads at each end of the indent lines were used to make visible markers allowing Raman microspectroscopy at $1\ \mu\text{m}$ intervals across the DEJ, while using the nanoindent markers for orientation and location. Functional DEJ width estimates were made based on results from nanoindentation and Raman microspectroscopy. DEJ width estimates ranged from $4.7 (\pm 1.2)\ \mu\text{m}$ to $6.1 (\pm 1.9)\ \mu\text{m}$ based on hardness and $4.9 (\pm 1.1)\ \mu\text{m}$ to $6.9 (\pm 1.9)\ \mu\text{m}$ based on modulus. DEJ width based on Raman peak intensity variations were $8.0 (\pm 3.2)\ \mu\text{m}$ to $8.5 (\pm 3.1)\ \mu\text{m}$ based on the phosphate peak, and $7.6 (\pm 3.2)\ \mu\text{m}$ to $8.0 (\pm 2.6)\ \mu\text{m}$ for C-H stretching mode. These estimates are in the range of DEJ width estimates reported using nanoindentation.

Copyright © 2010 R. R. Gallagher et al. This is an open access article distributed under the Creative Commons Attribution License, which permits unrestricted use, distribution, and reproduction in any medium, provided the original work is properly cited.

1. Introduction

The DEJ is a complex interfacial zone that joins two highly dissimilar calcified tissues, enamel and dentin. Enamel covers the coronal portion of a tooth and is primarily composed of a defective carbonate rich apatite arrayed in rods or prisms $4\text{--}5\ \mu\text{m}$ in diameter. These rods are oriented to intersect the DEJ almost perpendicularly and contain highly oriented long apatite crystals [1, 2]. Dentin is a calcified tissue that is compositionally similar to bone and is based on collagen reinforced with apatite. Dentin underlies enamel and is composed of a series of dentin tubules approximately $1\ \mu\text{m}$ in diameter. These tubules contain fluid and odontoblastic cellular processes that are surrounded by columnar-like peritubular dentin cylinders approximately $0.5\text{--}1\ \mu\text{m}$ thick. The mineral component of peritubular dentin contains randomly oriented apatite crystallites [3]. The mechanical behavior of

dentin is dominated by the behavior of intertubular dentin [4–8].

The DEJ plays a critical role in enhancing the biomechanical integrity and resistance to fracture [9, 10]. It has been found that the DEJ is more resistant to acid attacks [11] and crack propagation than is enamel [9, 12, 13]. The DEJ also has been observed to display a remarkable ability to transfer loads between enamel and dentin such that cracks or fracture planes that are formed within enamel rarely propagate across the DEJ into the underlying dentin [9, 14].

The DEJ usually has been described as consisting of a series of $25\text{--}100\ \mu\text{m}$ wide scallops, whose convexities are directed towards dentin and whose concavities are directed towards enamel [1, 2]. These scallops are further subdivided into a series of smaller microscallop, which contain finer structures [15].

Methods used to understand the complex hierarchical structure of calcified tissues and interfaces including dentin and the DEJ have recently been reviewed [14]. Large variations in width estimates of the DEJ have been reported in the literature. A variety of mechanical testing equipment, with increasingly smaller sampling sizes, has been used to estimate functional DEJ width based on its mechanical properties. Microhardness indentation profiles across the DEJ suggest that a broad gradation in mechanical properties exists [9]. Studies using Vickers microhardness measurements estimated the width of this interface as being between 27 to 100 μm [16]. Lin [17] and Lin and Douglas [9] determined a functional DEJ width in the range of 50 to 100 μm . They reported that their functional width estimate was considerably wider than its optical presentation. The apparent discrepancy among these measures may reflect a graded functional transition zone indicative of the DEJ region. Wang and Weiner reported a functional transition zone width on the order of 200 μm using a Moiré fringe technique on human teeth [18]. Nanoindentation testing yielded narrower DEJ width estimates. Fong et al. [13] employed nanomechanical testing and reported DEJ width estimates in the range of 15 to 25 μm , while Marshall et al. [12] used similar technology and estimated a functional DEJ width of 11 to 13 μm . Habelitz et al. [19] employed a nanoscratch technique and reported a very narrow linearly varying transitional zone of 1–3 μm . Balooch et al. [20] used AFM-based force modulation to measure the dynamic viscoelastic properties of the DEJ region and estimated DEJ width at 2 to 3 μm .

The observations that the mechanical properties of the DEJ exhibit a broad transitional behavior stand in contrast with high-resolution imaging. Studies have indicated that a very narrow interfacial zone, if any, exists between mantle dentin and enamel [21]. Data derived from light microscopy, and scanning and transmission electron microscopy, and atomic force microscopy suggest that the margins of the DEJ are sharply demarcated and that the interface is narrow [9, 12, 15, 16].

The small size of the DEJ, coupled with our inability to isolate this material, has made it a difficult tissue to study using conventional mechanical testing techniques. To date, bulk property measurements of the DEJ have not been obtained because conventional tensile, compressive and shear testing of the extremely small samples could produce complex geometries and nonuniform stress distributions. Pioch and Stachle [22] examined the shear strength of human and bovine teeth in the region of the DEJ and reported mean values of 39 MPa and 37.4 MPa, respectively. They reported that the fractures that occurred within dentin were not observed to occur at the DEJ, an indication of the scaling difficulties associated in working with this material.

Conventional morphological studies of the DEJ lack the ability to obtain chemically related information. Raman microspectroscopy is a technique to characterize the spatial distributions of organic and inorganic compounds with resolution on the order of 1 μm [23]. The Raman spectrum of enamel is dominated by peaks or bands attributed to the mineral apatite at 591, 961, and 1071 cm^{-1} . The

Raman spectrum of dentin indicates the presence of a larger proportion of organic compounds. C–H stretching bands at 2940 and 2880 cm^{-1} are more intense than those found in enamel. Amide I and III bands at 1670 and 1243 cm^{-1} also have been identified. These bands correlate with those found in the FT Raman spectra for bone and suggest a similar protein composition [24].

The hypothesis of this study was that width estimates of the DEJ based on compositional changes in the organic and mineral content are related to the mechanical properties changes determined by nanoindentation.

2. Materials and Methods

2.1. Sample Preparation. Five recently extracted noncarious human third molars were collected from the UCSF Oral Surgery clinic according to a protocol approved by the UCSF Institutional Committee on Human Research. Each tooth was maintained in a hydrated condition in physiologic saline solution (Hanks BSS) and gamma radiation sterilized according to a standard protocol [25]. Each tooth was sagittally sectioned parallel to its buccal-lingual surface with a water-cooled diamond saw and hand-polished through a graded series of SiC abrasive papers ending with 1200 grit and then final polishing with 0.05 μm alumina paste. Each specimen was ultrasonically cleaned for 60 seconds in ice-cooled deionized water between polishing steps to minimize the possibility of cross-contamination and scratching. Following final polishing, each sample was affixed to a magnetic backing plate with cyanoacrylate cement. The sample was air dried by blasts with clean, dry compressed air until all surface moisture was removed. Each sample was then positioned on the testing platen of the relevant testing machine. Nanoindentation testing and Raman microspectroscopy imaging were subsequently performed across the same section of the DEJ of each tooth, in the region of its central pit.

2.2. Nanoindentation Testing. An AFM-Triboscope system was used for imaging, nanomechanical testing and placing sample orientation markers. The AFM-Triboscope system consisted of a Nanoscope III (Veeco Probes, Santa Barbara, CA) with its standard head replaced by a Triboscope indenter system (Hysitron Inc., Minneapolis, MN). The coupled AFM-Triboscope system is a force generating and depth-sensing instrument [12, 26]. It is capable of imaging the area of testing before and following sampling. The Triboscope system consists of a three-plate capacitive force/displacement transducer in which a cube corner diamond tip is affixed via a central drive post to the middle plate. A voltage applied between the middle and the outer drive plates was used to generate an indentation force proportional to the square of the applied voltage. A feedback capacitive sensor determined indentation depth by sampling the feedback voltage. The system was capable of producing load-displacement curves at precisely selected locations with indentation loads ranging from 1 to 15 000 μN . A 90°-cube corner diamond tip was used for all indentations. This tip was calibrated before and after testing and had a tip radius of 20 nm. A trapezoidal force loading profile with adjustments to maintain measurement

validity was used for each measurement with a peak load of 300 μN . Each indentation produced a load-deformation curve from which the reduced elastic modulus was calculated from the contact stiffness, S , defined as the slope of the linear portion of the force/displacement curve during unloading near the maximum load using the unloading portion of the curve based on the equation

$$E = \frac{\sqrt{\pi}}{2\sqrt{a}}S, \quad (1)$$

where a is the projected contact area between the tip and sample at the maximum load.

Hardness was calculated as the maximum force divided by the projected contact area between the tip and the sample at the maximum load, in accordance with the methods of Doerner and Nix [27]

$$H = \frac{F_{\max}}{a}. \quad (2)$$

The same tip was used for imaging, nanomechanical testing and placing optically visible sample orientation markers. These markers were subsequently used to locate and orient the sample during Raman microspectroscopy.

In three of the samples, a single line of nanoindentation points, each having a length of at least 50 μm , was placed across the DEJ at 2 μm intervals to prevent interference with adjacent indentations. In the remaining two samples, two parallel lines of nanoindentation points, each with a length of at least 50 μm , were placed across the DEJ in opposite directions. All lines were made perpendicular to the DEJ, and oriented so that their midpoint was roughly coincident with the expected middle of the DEJ. Trial indentation lines of greater overall lengths were placed across the DEJ to ensure baseline modulus and hardness levels were achieved in both enamel and dentin. At the start of each indentation line, two indentation points were placed under maximal indentation load. A single indentation point was similarly placed at the end of each line. These terminal points were used as orientation markers as they were visible with the optical microscopes of both the AFM-Triboscope and the Raman microspectroscope. Figure 1 shows an AFM image of the DEJ with the orientation markers (Figure 1(a)) and typical spectra from the enamel and dentin on either side of the DEJ (Figure 1(b)).

Plots of hardness and modulus versus location were made. An estimate of the functional width of the DEJ was then made for each indentation line according to the statistical methods described below.

2.3. Raman Microspectroscopy. Raman microspectroscopy was used to characterize the mineralized matrix of dentin. It is a noncontact nondestructive technique that identifies and quantifies the functional groups that are present. An HR-800 Raman microspectrophotometer (Jobin Yvon, Horiba, France) was used to define the Raman spectra of enamel, dentin, and DEJ, as well as provide an estimate of the compositional width of the DEJ based on mineral and organic content differences. The HR-800 Raman microspectrophotometer uses monochromatic radiation emitted by

an He-Ne laser having a wavelength of 632.8 nm and operating at 20 mW of power before entrance optics. The spot size is on the order of 0.5 μm . In repeated tests we found that with 20 mW focused on 0.5 μm spot on dentin no significant change in the peak intensity or shape was observed with exposure times up to several minutes. Spectra were measured at 1 μm increments along lines across the DEJ in the same manner as for nanoindentation testing, yielding compositional information at half the sampling incremental distance of the nanoindentation study. Thus 50 spectra were obtained along each line of each specimen studied, and two or three lines were examined per specimen, so that 100–150 spectra per sample were obtained. Raman microspectroscope imaging lines were oriented to coincide with the orientation points placed in the sample by the AFM using the microspectroscope's 50x objective lens. The line of Raman spectra was offset laterally by 5 μm to avoid disturbances that might arise from the plastic deformation induced by the indents. The sample was scanned using a 30-second acquisition time for each Raman measurement point. Spectra were acquired for the phosphate (PO_4^{3-}) band at 960 cm^{-1} and the C–H stretching mode at 2940 cm^{-1} in three of the samples. The C–H stretching mode was chosen for two reasons as described in our earlier work [28]: (1) it had the potential to detect differences in noncollagenous proteins likely to be found in enamel or the DEJ as well as collagen in the dentin and (2) because the luminescence at the 2900 cm^{-1} band is much smaller than at other organic band locations (1660 near amide I, 1442, and 1200 cm^{-1} near amide III). Thus the background could be subtracted more accurately due to better signal-to-noise ratio. These constituted functional groups from the mineral (phosphate) and organic constituents, respectively. In one sample, spectra were acquired for only the phosphate band. One sample that received nanomechanical testing was not examined by Raman spectroscopy because of technical difficulties. Plots of PO_4^{3-} and C–H stretch intensity versus location were made. An estimate of the compositional DEJ width was then determined for each imaging line using the statistical methods described below. The results were compared to each other and to the nanomechanical results.

2.4. Statistical Analysis. To avoid the arbitrariness of estimating DEJ width by viewing graphed data, two statistical methods were developed using the SAS programming language. For each method, an algorithm was developed to select data inflection points based on deviations from linear models of the nanomechanical and Raman response of dentin and enamel. An inflection point was defined as being the first data point that varied significantly from the linearly modeled response. Inflection points defined the dentin-DEJ and DEJ-enamel borders. DEJ width was defined as the distance between these inflection points.

For the first method, nanoindenter and Raman data for dentin and enamel were defined to behave as linear models. To detect the dentin-DEJ junction, the algorithm was defined to begin at the dentin end of the data and move inward towards the DEJ. Each point was considered in turn beginning with the fourth data point. For each

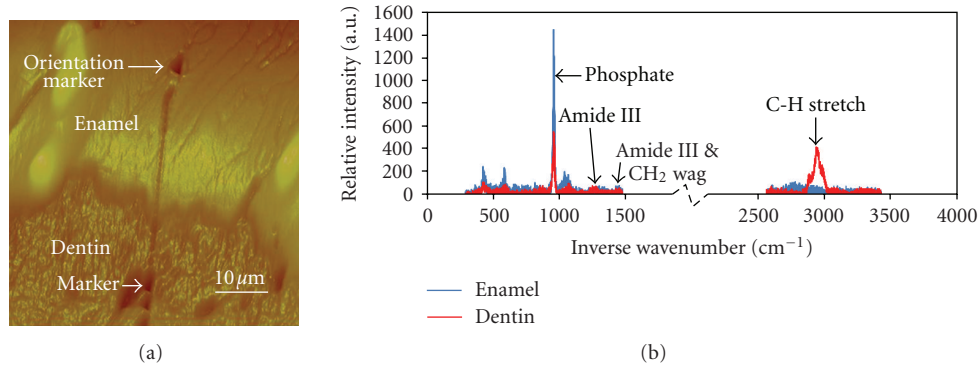


FIGURE 1: DEJ region. (a) An AFM image showing enamel and dentin with line of indents and orientation markers. (b) Typical spectra for regions of interest from enamel (blue) and dentin (red) near the DEJ.

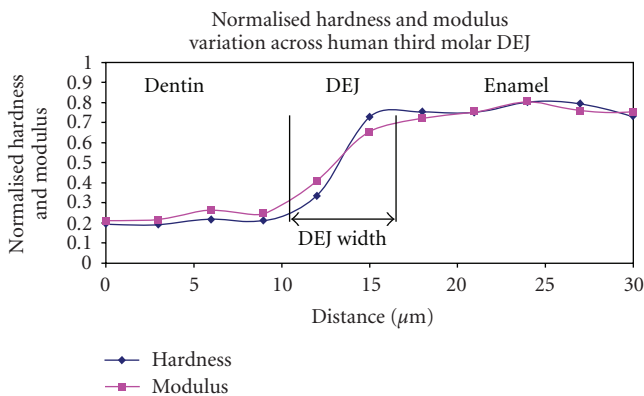


FIGURE 2: Typical normalized hardness and modulus variations along a line oriented to perpendicularly cross the DEJ. The hardness and modulus DEJ width estimates in this sample were both $8 \mu\text{m}$.

point considered, the algorithm determined if the point and the preceding three points were less than the value of the prior cut point, and if the following three points exceeded the value of the post cut point. The first such point under consideration that detected a difference was considered the dentin-DEJ inflection point. The DEJ-enamel inflection point, or where the junction “ends” and enamel “begins”, was similarly determined.

The second method for estimating DEJ width was based on detecting differences from linear models describing the DEJ’s nanomechanical and Raman behaviors. In this approach, mean values for the response of dentin and enamel were initially determined for each data line. These values were used to identify the construction midpoint of the DEJ. The construction midpoint was calculated as the middle of the difference between the mean response values of dentin and enamel. The data points located immediately on each side of the construction midpoint were identified. These points were used to fit a linear model describing the DEJ’s behavior.

The linear model of the DEJ’s behavior was used for statistical testing to estimate the dentin-DEJ and DEJ-enamel borders. In this approach, each point was sequentially

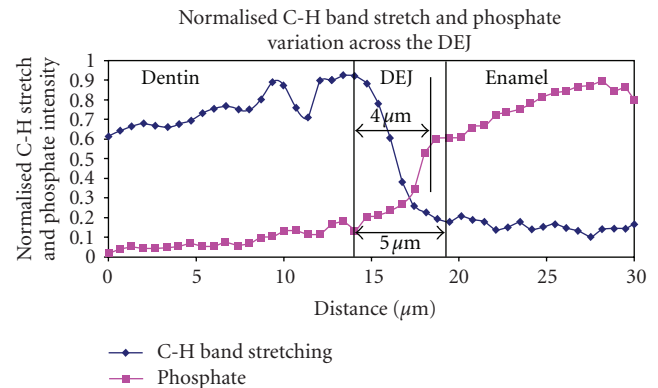


FIGURE 3: Typical normalized micro-Raman C–H stretch (2900 cm^{-1}) and phosphate band (960 cm^{-1}) peak intensity variations along a line oriented to cross the DEJ at a perpendicular angle. In this sample, DEJ width was estimated at $4 \mu\text{m}$ based on the peak phosphate band stretch intensity variation. Peak C–H stretching estimated DEJ width at $5 \mu\text{m}$.

examined to determine if it was within the eighty percent confidence interval of the predicted value. The first value falling beyond this range was defined as being an inflection point. The other inflection point was similarly determined. The width of the DEJ was calculated as the distance between these inflection points.

3. Results

Typical curves for normalized hardness, modulus, and intensities of the C–H stretch and phosphate band data are shown in Figures 2 and 3.

Mineral content was found to decrease monotonically from enamel to dentin, while organic content increased monotonically. Functional and compositional DEJ width estimates are tabulated in Table 1. DEJ width estimates based on hardness were $6.1 (\pm 1.9) \mu\text{m}$ according to statistical method 1 and $4.7 (\pm 1.2) \mu\text{m}$ according to statistical method 2. DEJ modulus width estimates were $6.9 (\pm 1.9) \mu\text{m}$ for method 1 and $4.9 (\pm 1.1) \mu\text{m}$ for method 2, respectively. Tests of statistical difference between the mean widths as

TABLE 1: Nanoindentation and Raman microspectroscopy DEJ width estimates.

Measure	Observations	Statistical method 1		Statistical method 2	
		Mean (μm)	Std Dev (μm)	Mean (μm)	Std Dev (μm)
Hardness	7	6.1	1.9	4.7	1.2
Modulus	7	6.9	1.9	4.9	1.1
Raman 960	4	8.0	3.2	8.5	3.1
Raman 2900	3	7.6	3.2	8.0	2.6

TABLE 2: Summary statistics for combined measures DEJ width estimates.

Measure	Method 1 (μm)				Method 2 (μm)			
	Mean	Std. Err.	95% CI	Std. Dev. ⁽¹⁾	Mean	Std. Err.	95% CI	Std. Dev. ⁽¹⁾
Indentation	6.4	0.63	4–9	1.8	4.6	0.60	2–7	1.1
Raman	7.8	0.86	4–11	2.9	8.3	0.74	5–12	2.7

⁽¹⁾The Standard Deviation (Std. Dev.) was computed using measured DEJ widths. Other measures were computed using widths estimates that employed a linear model which adjusted for multiple measurements on the same tooth and combined measurements using the same instrumentation device (hardness and modulus or Raman 960 cm^{-1} and 2900 cm^{-1} peaks).

estimated by either indentation method for each statistical method indicated that the indentation results for hardness and modulus yielded similar and consistent estimates of the functional DEJ width. Since no statistical difference between the results was noted, we combined the indentation width estimates into a single “technique” width estimate of 6.4 (Standard Error \pm 0.63, 95% confidence interval: 4–9) μm according to method 1 and 4.6 (Standard Error \pm 0.60, 95% confidence interval: 2–7) μm for method 2. These estimates from combined methods were provided by a general linear model that adjusted for multiple measures made on the same tooth and are contained in Table 2.

DEJ functional width estimates based on Raman-microspectroscopy yielded a phosphate band estimate of 8.0 (\pm 3.2) μm according to method 1 and 8.5 (\pm 3.1) μm according to method 2. The C–H stretching mode width estimates were 7.6 (\pm 3.2) μm for method 1 and 8.0 (\pm 2.6) μm for method 2. Tests of statistical difference between mean DEJ width estimates for the two Raman methods showed no significant difference. As with the indentation data, we combined the two Raman estimates into a single microspectroscopy estimate of 7.8 (Standard Error \pm 0.86) μm with a 95% confidence interval of 4–11 μm according to method 1. The combined estimate (Table 2) provided by method 2 is 8.3 (Standard Error \pm 0.74) μm with a 95% confidence interval of 5–12 μm .

DEJ width estimates based on the two types of measurements, nanoindenter and Raman microspectroscopy, did not show a statistically significant difference with method 1, but did show a statistically significant difference according to method 2 (P -value = .035 from SAS proc mixed). Taking the lower 95% confidence interval of the smallest estimate and the upper 95% confidence interval of the largest estimate gave a conservative estimate of the width of the DEJ for each instrumentation method based on multiple measurements. For the indenter data, this range was 2–9 μm ; for the Raman data it was 4–12 μm .

4. Discussion

The chemical composition and the mechanical behavior of the DEJ region were characterized using Raman microspectroscopy and nanoindentation testing. Studies using nanoindentation revealed variations of microstructure in calcified tissues such as enamel [29, 30] and the DEJ [15]. The coupled AFM-Triboscope system allowed site-specific mechanical property measurements to be made, affording estimates of the functional DEJ width by spatially mapping the nanomechanical response across the junction. Both instruments tested the same areas of each sample and allowed us to compare and contrast the results. Our current work found consistent mean functional DEJ width estimates using hardness and modulus of between 4.7 and 6.9 μm . The nanoindentation DEJ width estimates based on hardness data were somewhat narrower than estimates obtained using modulus data, although the difference was not statistically significant. Hardness and modulus were found to vary linearly across the DEJ and were highest in enamel. This was in agreement with earlier work [9, 12]. The nanomechanical width estimates were found to be independent of testing direction. The nanomechanical results represent a refinement in the functional width estimates from previous nanoindentation results [12, 13]. This may result from the use of an extremely sharp cube corner tip that allowed shallower indentation depths and smaller sampling volumes to be made. In our study, we also used the nanoindenter to place optically visible sample orientation markers that allowed comparison of the nanoindentation and Raman microspectroscopy data.

No unique Raman signature was observed for the DEJ. Relatively linear variations in the Raman profiles for the phosphate and C–H stretching mode peaks were observed across the DEJ. The phosphate peak, an indication of the mineral content present, was found to be highest in enamel and lowest in dentin. The converse was observed for the

C–H stretching mode, an indication of the protein content variation across this region.

Estimates of DEJ width based on Raman microspectroscopy produced results that were consistent and greater (by approximately $1\ \mu\text{m}$) than those determined from nanomechanical property profiles. The variance of the spectroscopy width estimates was roughly twice that found using nanomechanical testing. The effect of testing direction was not determined for micro-Raman width estimates due to insufficient data. The results indicate that the nanomechanical DEJ width estimates were narrower and less variable than those using Raman microspectroscopy.

The spectroscopic and indentation data showed monotonic mechanical and spectroscopic property variations across the DEJ. While it is possible that the observed variation in properties could represent the actual behaviors, it is more likely that what we observed is actually a superimposition or averaging of the dentin and enamel properties.

The DEJ is a highly irregular and undulating junction. It has a three-level structure consisting of 25–100 μm scallops that are subdivided by 2–5 μm microscallops and smaller scale structures. Indentations and spectroscopy performed on such a three-dimensional structure may sample varying mixtures of the constituents bordering each side of the interface since sampling occurs over a finite volume. The greater the sampling volume, the higher the probability that sample mixing is occurring. Sample volumes consisting of two or more phases produce property measurements different from those of the bordering materials. Testing modalities that minimize sampling depth, width, and volume produce more accurate material property measurements having greater spatial resolution. For indentation testing, narrower DEJ width estimates are dependent upon minimizing indentation depth via the use of sharper indentation tips since they lead to decreased sample mixing and narrower step widths.

In this study, we attempted to control the effect of the undulating scalloped architecture of the DEJ by orienting the sampling lines to cross the DEJ at a perpendicular angle. It is likely that sampling lines also crossed the scalloped DEJ at other angles, leading to increases in the size and variability of the functional DEJ width estimates. Additionally, since approximately 5 μm of lateral offset between paired indentation and spectroscopic sampling lines were made, the material sampled by each method was slightly different.

Differences in sampling volume exist between Raman microspectroscopy and nanoindentation testing. The sampling volume we used for Raman microspectroscopy was on the order of $1\ \mu\text{m}$. This is 4 to 20 times greater than the nanoindentation sample volumes that were used. The Raman sampling volume was less defined than the plastically deformed zone indicative of nanomechanical testing. These differences explain the greater variability observed in the spectroscopy results. Coupling the increased sample volumes for Raman imaging with the size of the DEJs microscallops; it is evident that sample mixing was occurring more often than for nanoindentation testing. It is likely that this is responsible for the narrower DEJ width estimates obtained from mechanical testing despite the fact that the sampling interval was twice as great.

5. Conclusions

No characteristic mechanical or spectroscopic properties were noted for the DEJ. DEJ width estimates of 6.1 to 6.9 μm based on nanomechanical testing, and 7.6 to 8.5 μm based on micro-Raman spectroscopic mapping were found for either statistical method used to analyze the results. DEJ width estimates were essentially independent of the statistical techniques employed. It is probable that the DEJ's undulating three-leveled architecture is responsible for many of the observed behaviors. Further studies involving larger sample sizes could improve our understanding of this variability. Our results are in line with earlier work [14] and represent a mechanism for linking the physical properties to their composition.

Acknowledgments

The authors would like to thank Dr. Sunita Ho and Dr. Stefan Habelitz for assistance and helpful discussions. This work was performed at Lawrence Livermore National Laboratory under the auspices of the U.S. Department of Energy and was supported by the U.S. Public Health Service through National Institutes of Health/National Institute of Dental and Craniofacial Grants K16 DE00386 (R.R. Gallagher) and R01 DE 13029.

References

- [1] A. R. Ten Cate, *Oral Histology: Development, Structure, and Function*, Mosby, St. Louis, Mo, USA, 4th edition, 1994.
- [2] S. N. Bhaskar, Ed., *Orban's Oral Histology and Embryology*, Mosby Year Book, Chicago, Ill, USA, 11th edition, 1990.
- [3] G. W. Marshall Jr., "Dentin: microstructure and characterization," *Quintessence International*, vol. 24, no. 9, pp. 606–617, 1993.
- [4] J. H. Kinney, M. Balooch, G. W. Marshall Jr., and S. J. Marshall, "A micromechanics model of the elastic properties of human dentine," *Archives of Oral Biology*, vol. 44, no. 10, pp. 813–822, 1999.
- [5] D. Arola, J. A. Rouland, and D. Zhang, "Fatigue and fracture of bovine dentin," *Experimental Mechanics*, vol. 42, no. 4, pp. 380–388, 2002.
- [6] S. T. Rasmussen, R. E. Patchin, D. B. Scott, and A. H. Heuer, "Fracture properties of human enamel and dentin," *Journal of Dental Research*, vol. 55, no. 1, pp. 154–164, 1976.
- [7] S. T. Rasmussen and R. E. Patchin, "Fracture properties of human enamel and dentin in an aqueous environment," *Journal of Dental Research*, vol. 63, no. 12, pp. 1362–1368, 1984.
- [8] N. Iwamoto and N. D. Ruse, "NTP specimen fracture toughness test applied to human dentin," in *Proceedings SEM Annual Conference and Exposition on Experimental and Applied Mechanics*, Society of Experimental Mechanics, pp. 90–91, Portland, Ore, USA, 2001.
- [9] C. P. Lin and W. H. Douglas, "Structure-property relations and crack resistance at the bovine dentin-enamel junction," *Journal of Dental Research*, vol. 73, no. 5, pp. 1072–1078, 1994.
- [10] V. Imbeni, J. J. Kruzic, G. W. Marshall Jr., S. J. Marshall, and R. O. Ritchie, "The dentin-enamel junction and the fracture of human teeth," *Nature Materials*, vol. 4, no. 3, pp. 229–232, 2005.

- [11] P. Tramini, B. Pélissier, J. Valcarcel, B. Bonnet, and L. Maury, "A Raman spectroscopic investigation of dentin and enamel structures modified by lactic acid," *Caries Research*, vol. 34, no. 3, pp. 233–240, 2000.
- [12] G. W. Marshall Jr., M. Balooch, R. R. Gallagher, S. A. Gansky, and S. J. Marshall, "Mechanical properties of the dentinoenamel junction: AFM studies of nanohardness, elastic modulus, and fracture," *Journal of Biomedical Materials Research*, vol. 54, no. 1, pp. 87–95, 2001.
- [13] H. Fong, M. Sarikaya, S. N. White, and M. L. Snead, "Nanomechanical properties profiles across dentin-enamel junction of human incisor teeth," *Materials Science and Engineering C*, vol. 7, no. 2, pp. 119–128, 2000.
- [14] J. L. Katz, A. Misra, P. Spencer, et al., "Multiscale mechanics of hierarchical structure/property relationships in calcified tissues and tissue/material interfaces," *Materials Science and Engineering C*, vol. 27, no. 3, pp. 450–468, 2007.
- [15] S. J. Marshall, M. Balooch, S. Habelitz, G. Balooch, R. R. Gallagher, and G. W. Marshall Jr., "The dentin—enamel junction—a natural, multilevel interface," *Journal of the European Ceramic Society*, vol. 23, no. 15, pp. 2897–2904, 2003.
- [16] S. N. White, M. L. Paine, W. Luo, et al., "The dentinoenamel junction is a broad transitional zone uniting dissimilar bioceramic composites," *Journal of the American Ceramic Society*, vol. 83, no. 1, pp. 238–240, 2000.
- [17] C. P. Lin, *Structure-function property relationships in the dentin-enamel complex and tooth restoration interface*, Ph.D. thesis, University of Minnesota, 1993.
- [18] R. Z. Wang and S. Weiner, "Strain-structure relations in human teeth using Moire fringes," *Journal of Biomechanics*, vol. 31, no. 2, pp. 135–141, 1997.
- [19] S. Habelitz, S. J. Marshall, G. W. Marshall Jr., and M. Balooch, "The functional width of the dentino-enamel junction determined by AFM-based nanoscratching," *Journal of Structural Biology*, vol. 135, no. 3, pp. 294–301, 2001.
- [20] G. Balooch, G. W. Marshall Jr., S. J. Marshall, O. L. Warren, S. A. S. Asif, and M. Balooch, "Evaluation of a new modulus mapping technique to investigate microstructural features of human teeth," *Journal of Biomechanics*, vol. 37, no. 8, pp. 1223–1232, 2004.
- [21] P. Bodier-Houllé, P. Steuer, J. M. Meyer, L. Bigeard, and F. J. G. Cuisinier, "High-resolution electron-microscopic study of the relationship between human enamel and dentin crystals at the dentinoenamel junction," *Cell and Tissue Research*, vol. 301, no. 3, pp. 389–395, 2000.
- [22] T. Pioch and H. J. Stachle, "Experimental investigation of the shear strengths of teeth in the region of the dentinoenamel junction," *Quintessence International*, vol. 27, no. 10, pp. 711–714, 1996.
- [23] M. Pelletier and M. J. Pelletier, *Analytical Applications of Raman Spectroscopy*, Blackwell Science, Malden, Mass, USA, 1999.
- [24] P. Hendra, C. Jones, and G. Warnes, *Fourier Transform Raman Spectroscopy: Instrumentation and Chemical Applications*, Ellis Horwood Series in Analytical Chemistry, Ellis Horwood, New York, NY, USA, 1991.
- [25] J. M. White, H. E. Goodis, S. J. Marshall, and G. W. Marshall Jr., "Sterilization of teeth by gamma radiation," *Journal of Dental Research*, vol. 73, no. 9, pp. 1560–1567, 1994.
- [26] M. Balooch, I.-C. Wu-Magidi, A. Balazs, et al., "Viscoelastic properties of demineralized human dentin measured in water with atomic force microscope (AFM)-based indentation," *Journal of Biomedical Materials Research*, vol. 40, no. 4, pp. 539–544, 1998.
- [27] M. F. Doerner and W. D. Nix, "A method for interpreting the data from depth-sensing indentation instruments," *Journal of Materials Research*, vol. 1, pp. 601–609, 1986.
- [28] K. A. Schulze, M. Balooch, G. Balooch, G. W. Marshall Jr., and S. J. Marshall, "Micro-Raman spectroscopic investigation of dental calcified tissues," *Journal of Biomedical Materials Research Part A*, vol. 69, no. 2, pp. 286–293, 2004.
- [29] S. Habelitz, S. J. Marshall, G. W. Marshall Jr., and M. Balooch, "Mechanical properties of human dental enamel on the nanometer scale," *Archives of Oral Biology*, vol. 46, pp. 173–183, 2001.
- [30] S. Park, D. H. Wang, D. Zhang, E. Romberg, and D. Arola, "Mechanical properties of human enamel as a function of age and location in the tooth," *Journal of Materials Science: Materials in Medicine*, vol. 19, no. 6, pp. 2317–2324, 2008.